ESE-ENDOR Study and DFT Calculations on Oxovanadium Compounds: Effect of Axial Anionic Ligands on the ^{51}V Nuclear Quadrupolar Coupling Constant

Constantino P. Aznar,[†] Yiannis Deligiannakis,*[,‡] Evangelos J. Tolis,[§] Themistoklis Kabanos,[§] Marcin Brynda,[†] and R. David Britt*[,†]

Department of Chemistry, University of California, Davis, California, 95616, Department of Environmental and Natural Resources Management, Laboratory of Physical Chemistry, University of Ioannina, Pyllinis 9, 30100 Agrinio, Greece, and Department of Chemistry, Section of Inorganic and Analytical Chemistry, University of Ioannina, 451 10 Ioannina, Greece

Received: November 21, 2003; In Final Form: February 27, 2004

High-frequency electron spin echo-electron nuclear double resonance (ESE-ENDOR) spectroscopy is applied to oxovanadium VO^{2+} complexes of Hcapca in the form of *trans*-[VOX(capca)] and to H_2capcah in the form of *cis*-[VOX(Hcapcah)], where X = Cl^- or SCN^-. Nuclear quadrupolar coupling constants (nqcc), which are unobtainable by conventional continuous-wave electron paramagnetic resonance (CW-EPR), were measured and reported in terms of $\mathbf{P}_{||}$ ($\mathbf{P}_{||} = 3e^2qQ/84$ for $I = {}^7/_2$). $\mathbf{P}_{||}$ values for *trans*-[VOCl(capca)] and *trans*-[VOSCN-(capca)] were calculated to be −0.18 and −0.21 MHz, respectively. In the cases of *cis*-[VOCl(Hcapcah)] and *cis*-[VOSCN(Hcapcah), $\mathbf{P}_{||}$ values were calculated to be −0.35 and −0.45 MHz, respectively. The experimental results are supported by DFT calculations of quadrupolar and hyperfine couplings for various oxovanadium compounds, including the cis and trans complexes studied by ESE-ENDOR. The charged ligands, coordinated axially trans to the oxo bond, reduce the electric field gradient along the V═O bond, thereby decreasing the observed magnitude of the nuclear quadrupolar coupling constants relative to those of the comparable cis compounds. This experimental finding is confirmed by quantum mechanical calculations. Although the absolute values of quadrupolar splittings cannot be calculated with acceptable accuracy, the observed experimental trends are very well reproduced. Thus, the complementary use of DFT and pulsed-ENDOR is a promising methodology for the study of biologically relevant vanadyl compounds.

Introduction

The vanadyl ion, (VO^{2+}), has been studied by electron paramagnetic resonance (EPR) techniques for both naturally occurring vanadoproteins and vanadyl-substituted systems.[1,2] It has been used as an EPR probe because it can not only substitute for various divalent metals but it can also mimic metal interactions between Mg(II) and nucleotides.[3] The interest in oxovanadium compounds has been influenced by the discovery of vanadium-containing enzymes[4−6] and the insulin-mimetic activity of vanadium complexes in mammals.[7−10] Some oxovanadium compounds have also been found to have an antitumorogenic effect.[11] Generally, compounds of vanadyl ions are five- or six-coordinate, with the axial V═O bond defining the *z* direction of the molecular geometry. Their CW-EPR spectra are characterized by eight anisotropic lines resulting from the interaction of the ^{51}V ($I = {}^7/_2$) nuclear spin with the single unpaired electron spin ($S = {}^1/_2$).

One can obtain structural information from the *g* and hyperfine principal values (A_{ii}) derived from the spectra. The correlation of g_z and A_{zz} provides clues to the identity of the equatorial ligands.[2,12−13] The contributions of the weakly bound axial ligands, however, are indiscernible in the CW-EPR spectra. Electron spin echo envelope modulation (ESEEM) spectroscopy and electron nuclear double resonance (ENDOR) spectroscopy are also used, mainly to characterize ligands by measuring their hyperfine coupling and quadrupolar constants.[1,14a,b−16] ESEEM in particular is useful in the identification of equatorial nitrogen ligands.[14b] Recently, ESEEM was also successfully used to detect axial nitrogen ligands.[14a,b]

Qualifying and quantifying the contribution of axial ligands is important because they may provide a better picture of how vanadium-containing compounds and proteins function. One method of investigating the effect of axial ligands is through the application of high-frequency electron spin echo-electron nuclear double resonance (ESE-ENDOR) targeting the ^{51}V nucleus as demonstrated by Grant et al.[17,18] The measurement of the nuclear quadrupolar coupling constant (nqcc) showed that the nqcc of ^{51}V is sensitive to the type of neutral axial ligand.[17] In addition, the magnitude of the nqcc was found to be characteristic of the geometry of five-coordinate VO^{2+} compounds.[18] Following these results, in this work we apply ESE-ENDOR spectroscopy to measure the nqcc of *trans*-[VOX(capca)] and *cis*-[VOX(Hcapcah)], where X = Cl^- or SCN^-. A previous study showed that the trans form of Hcapca with negatively charged ligands has a parallel hyperfine component, A_z, which is 16% less than for those complexes with simalar equatorial ligand donor sets.[12,19] In the present work based on ESE-ENDOR spectroscopy, we show that the nqcc values of *trans*-[VOX(capca)] and *cis*-[VOX(Hcapcah)] were substantially reduced relative to the nqcc values of some five-coordinate compounds previously studied. Moreover, *trans*-[VOCl(capca)] and *trans*-[VOSCN(capca)] were found to have

* To whom correspondence should be addressed. E-mail: rdbritt@ucdavis.edu; ideligia@cc.uoi.gr.
† University of California.
‡ Department of Environmental and Natural Resources Management, University of Ioannina.
§ Department of Chemistry, University of Ioannina.

10.1021/jp037560f CCC: $27.50
Published on Web 04/15/2004

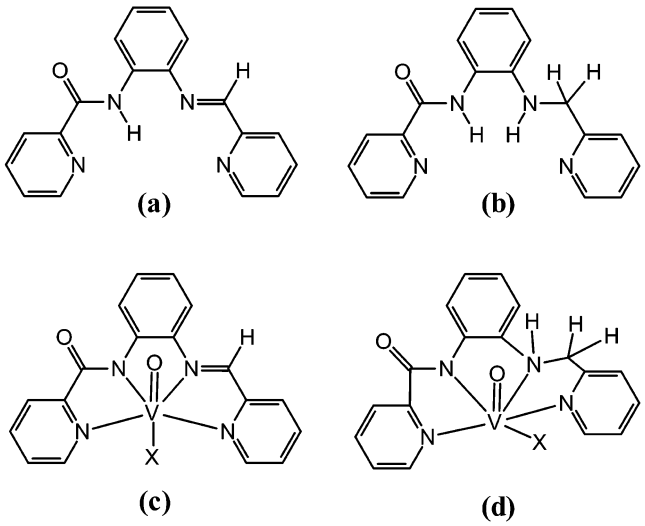

Figure 1. Chemical structures of (a) Hcapcah, (b) H_2capcah, (c) *trans*-[VOX(capcah)], and (d) *cis*-[VOX(Hcapcah)]. Atom X represents Cl^- or SCN^-.

smaller nqcc values than *cis*-[VOCl(Hcapcah)] and *cis*-[VOSCN(Hcapcah)]. In any case, axial ligands, charged or uncharged, influence the electric gradient and therefore the nqcc of ^{51}V. This work demonstrates that ^{51}V ESE-ENDOR is an alternative spectroscopic tool for investigating weak metal−axial ligand interaction.

Quantum Mechanical Calculations. Density functional theory (DFT) has been proven to be an accurate predictive tool not only for the calculation of molecular geometries but also for the computation of physical and spectroscopic properties of molecules such as NMR shifts, hyperfine and dipolar coupling constants, and nuclear quadrupolar couplings. In this paper, we attempt to make systematic calculations of the NQR and EPR parameters of a series of model oxovanadium complexes, which were independently studied by ESE-ENDOR spectroscopy. The molecular geometries were optimized in the gas phase using DFT theory with a hybrid B3LYP functional, including Becke's three-parameter nonlocal exchange potential and the nonlocal correlation functional of Lee, Yang, and Parr. The same method was used for the calculations of nuclear quadrupole and hyperfine interactions. An additional set of calculations of the hyperfine tensor was also performed with the half-and-half hybrid BHandHLYP functional. Various basis sets were tested in order to understand the influence of the quality of the basis set on the accuracy of the calculated values of the EPR and NQR parameters. The optimized geometries for model compounds were verified for the real minima by a careful analysis of the calculated vibrational frequencies (second derivative of the energy). DFT calculations were carried out using the Gaussian 98 package[20a] and the ADF program.[20b] The representations of the molecular structures were generated with the MOLEKEL program.[21]

Whereas a majority of quantum mechanical calculations of quadrupolar interactions deal with diamagnetic molecules, very few calculations have been reported in the literature for the paramagnetic species. Recently, theoretical work focused on the quadrupolar interaction in oxygen, sulfur and germanium,[22] bromine,[23] magnesium,[24] and beryllium.[25] Quadrupolar splitting parameters were also theoretically investigated in synthetic iron−oxo complexes.[26] Calculations of the quadrupolar interaction for ^{14}N in various organic and inorganic compounds[27] are abundant in the literature. Very recently, we have shown the usefulness of DFT theory as a predictive tool for the assignment of the experimental quadrupolar couplings on the distinct amino and imino nitrogens in the imidazole ring of the synthetic model for the covalently ring-linked tyrosine-histidine in the heme-copper oxidases.[28]

In a recent paper, Saladino and Larsen[29] described DFT calculations on paramagnetic oxovanadium complex with imidazole carried out with the zeroth-order relativistic approximation (ZORA) implemented in the Amsterdam Density Functional (ADF) package. To the best of our knowledge, this is the first attempt at the calculations of the quadrupolar parameters of the paramagnetic vanadium (IV) complex. Modern EPR techniques are able to provide the spectroscopist with the experimental values of quadrupolar couplings and hyperfine parameters in paramagnetic vanadium complexes. Thus it is an important topic because it provides the theoretical predictions for the quadrupolar interactions in these species and may be used to test the accuracy and validity of the available quantum mechanical methods in order to support the experimental EPR results.

The electric field gradient (EFG) is a fundamental ground-state property of the molecules, which by interaction with the quadrupolar moment of the nucleus gives rise to the quadrupolar splittings of the nuclear energy levels. From the experimentally determined transitions between these levels, the EFG can be calculated. The EFG directly reflects the electronic charge distribution in the vicinity of the nucleus and thus is extremely sensitive to the geometrical and electrostatical changes around the nuclei. The traceless electric field gradient tensor elements in Cartesian coordinates are defined as

$$V_{ij} = \frac{\partial^2 \Phi}{(\partial x_i \partial x_j)}|_0 \frac{-1}{3}\delta_{ij}\Delta\Phi|_0 \tag{1}$$

where

$$\Phi(r) = \int \frac{\rho(r')}{|r - r'|}\,\mathrm{d}r \tag{2}$$

Thus

$$v_{ij} = \rho(r)\left(\frac{-3x_i x_j}{r^5} - \frac{\delta_{ij}}{r^3}\right)\mathrm{d}r \tag{3}$$

and traceless EFG tensor elements are related to the quadrupolar coupling constant C_q by

$$C_q = \frac{e^2 Q\langle q_{zz}\rangle}{h} \tag{4}$$

The asymmetry parameter η is defined according to

$$\eta = \frac{\langle q_{xx}\rangle - \langle q_{yy}\rangle}{\langle q_{zz}\rangle} \tag{5}$$

where $e\langle q_{xx}\rangle$, $e\langle q_{yy}\rangle$, and $e\langle q_{zz}\rangle$ are the principal components of the electric field gradient tensor. To convert the q_{zz} output from atomic units (au) to the ^{51}V quadrupolar coupling constant, a value of $e^2Q/h = -12.32$ MHz was used. This corresponds to a quadrupolar moment Q of ^{51}V equal to -0.052×10^{-24} cm^2.[30]

For the accurate computation of the EFG, the correlation must be included in the computational scheme, and the use of a rather large basis set is necessary. The accuracy of the computed EFG is also related to the contribution of the electronic core polarization and relativistic effects.[31,32]

Experimental Section

The synthesis of *trans*-[VOCl(capca)], *trans*-[VOSCN(capca)], *cis*-[VOCl(Hcapcah)], and *cis*-[VOSCN(Hcapcah)]

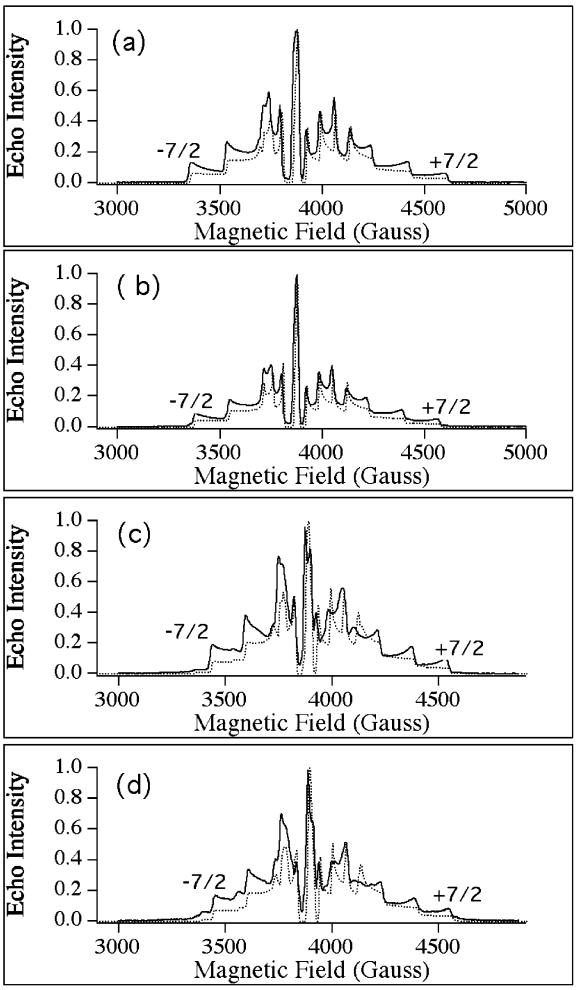

Figure 2. Two-pulse ESE-EPR field-swept spectra (—) for (a) *cis*-[VOCl(Hcapca)], (b) *cis*-[VOSCN(Hcapca)], (c) *trans*-[VOCl(capca)], and (d) *trans*-[VOSCN(capca)]. Experimental parameters are (a) $\nu_{mw} = 10.8928$ GHz, $\tau = 500$ ns; (b) $\nu_{mw} = 10.8830$ GHz, $\tau = 520$ ns; (c) $\nu_{mw} = 10.8958$ GHz, $\tau = 300$ ns; and (d) $\nu_{mw} = 10.9250$ GHz, $\tau = 290$ ns. For a and b, $\pi/2 = 100$ and $\pi = 200$ ns in duration, whereas for c and d, $\pi/2 = 50$ and $\pi = 100$ ns. Pertinent parameters used for simulation (• • •) are (a) $g_x = 1.983$, $g_y = 1.980$, $g_z = 1.951$, $A_x = 176$ MHz, $A_y = 165$ MHz, $A_z = 495$ MHz; (b) $g_x = 1.982$, $g_y = 1.981$, $g_z = 1.955$, $A_x = 160$ MHz, $A_y = 160$ MHz, $A_z = 471$ MHz; (c) $g_x = 1.981$, $g_y = 1.979$, $g_z = 1.949$, $A_x = 157$ MHz, $A_y = 145$ MHz, $A_z = 435$ MHz; and (d) $g_x = 1.981$, $g_y = 1.980$, $g_z = 1.949$, $A_x = 156$ MHz, $A_y = 144$ MHz, $A_z = 439$ MHz.

complexes (Figure 1) is described in detail elsewhere.[12,19] Samples were dissolved in a 7:3 mixture of methanol/ethanol to obtain 3−5 mM solutions depending on the complexes' solubility.

Pulsed-EPR experiments were performed on a laboratory-built spectrometer described previously.[33,34] ESE-detected EPR spectra were obtained using the two-pulse sequence $\pi/2-\tau-\pi-\tau-$echo. For ESE-ENDOR, the Davies ENDOR[35] sequence, $\pi-T-\pi/2-\tau-\pi-\tau-$echo, was used, where T designates the time when the radio-frequency (rf) pulse is applied. The π microwave (MW) pulse duration is typically 50−100 ns. An approximately 100W rf pulse is applied with 20 ms duration and is incremented by 0.2 MHz over the rf range. ESE-ENDOR spectra were collected at the edge of the $M_I = \pm 7/2$ parallel turning points of the field-sweep EPR as shown in Figure 2. All experiments were performed at an X-band frequency of 10.9 GHz and at a temperature of approximately 15 K.

DFT Methodology. To gain an insight into the usability of the DFT method for the EFG calculations of the vanadium complexes, we decided to carry out the theoretical investigations by using DFT theory as implemented in the Gaussian 98 package. In the preliminary stage, we have scanned the influence of different basis sets of increasing size on the calculated values of the quadrupolar and hyperfine interactions to choose the desired basis set for further calculations. This "calibrating" study was carried out on the simplest oxovanadium complex that was previously investigated by ESE-ENDOR spectroscopy in our laboratory and whose C_q value was experimentally determined.[36] As the first step, the geometry of the aqua VO complex $[VO(H_2O)_5]^{2+}$ was optimized. Once the optimized geometry was in hand, we successively tested the accuracy of the calculated C_q versus an experimental value with basis sets of increasing size.

In the second stage, for the calculations of the NQR and EPR parameters of our experimental systems studied by ESE-ENDOR, we have used the coordinates extracted from the available crystal structures. We have also constructed a series of model compounds, based on the minimum number of atoms, that mimic the conjugated systems of the studied complexes *cis*-[VOX(Hcapcah)] and *trans*-[VOX(capca)] ($X = Cl^-$, SCN^-) previously used for DFT calculations by Tolis et al.[12] To reduce the computational time, the aromatic groups were simply mimicked by double bonds. This approach was undertaken to determine if the calculations on the reduced models can be satisfactorily compared to the calculations on the real molecular systems.

Finally, we have also calculated the quadrupolar interaction for three oxovanadium complexes—VO(oep) (**2**), $VO(acac)_2$ (**3**), and VO(salen) (**4**)—that have already been studied by pulsed ENDOR spectroscopy and whose quadrupolar parameters were reported earlier.[18]

Molecular Structures and Geometry Optimizations. The geometries of the oxovanadium complexes used in this theoretical study are presented in Figure 3. The geometry of the aqua VO complex $[VO(H_2O)_5]^{2+}$ (**1**) was optimized at the B3LYP level with the 6-31g* basis set. The same procedure was used for the optimizations of the geometries of model complexes *cis*-M1-Cl (**5**), *trans*-M2-Cl (**6**), *cis*-M1-SCN (**7**), and *trans*-M2-SCN (**8**). Whereas model compounds containing the Cl^- ion were fully optimized, the optimization of the two remaining structures with the SCN^- ion was only partial because of the computational limitations. To achieve complete optimization, a small energy gradient is needed, but that requires an important grid and is computationally very expensive. From four experimentally investigated compounds, only three crystal structures of vanadium complexes *cis*-[VOCl(Hcapcah)] (**9**), *trans*-[VOCl-(capca)] (**10**), and *cis*-[VOSCN(Hcapcah)] (**11**) are available. To perform the calculations of the EFG and EPR tensors for the *trans*-[VOSCN(capca)] (**12**) complex on a realistic model, a partial optimization of its structure was also performed. Thus, the calculations of the EFG and EPR were realized on the parameters extracted from the crystal structures for complexes **2**−**4** and **9**−**11**, on fully optimized structures **5**−**6**, and on partially optimized structures of **8** and **12**.

Results

ESE-detected EPR spectra of *trans*-[VOCl(capca)], *trans*-[VOSCN(capca)], *cis*-[VOCl(Hcapca)], and *cis*-[VOSCN(Hcapca)] are shown in Figure 2. All spectra are typical for VO^{2+} complexes. Also shown by dotted lines are simulations calculated using the QPOW program.[37−39] The small bumps at the edges of the spectrum of the field-swept spectra of *trans*-[VOX-

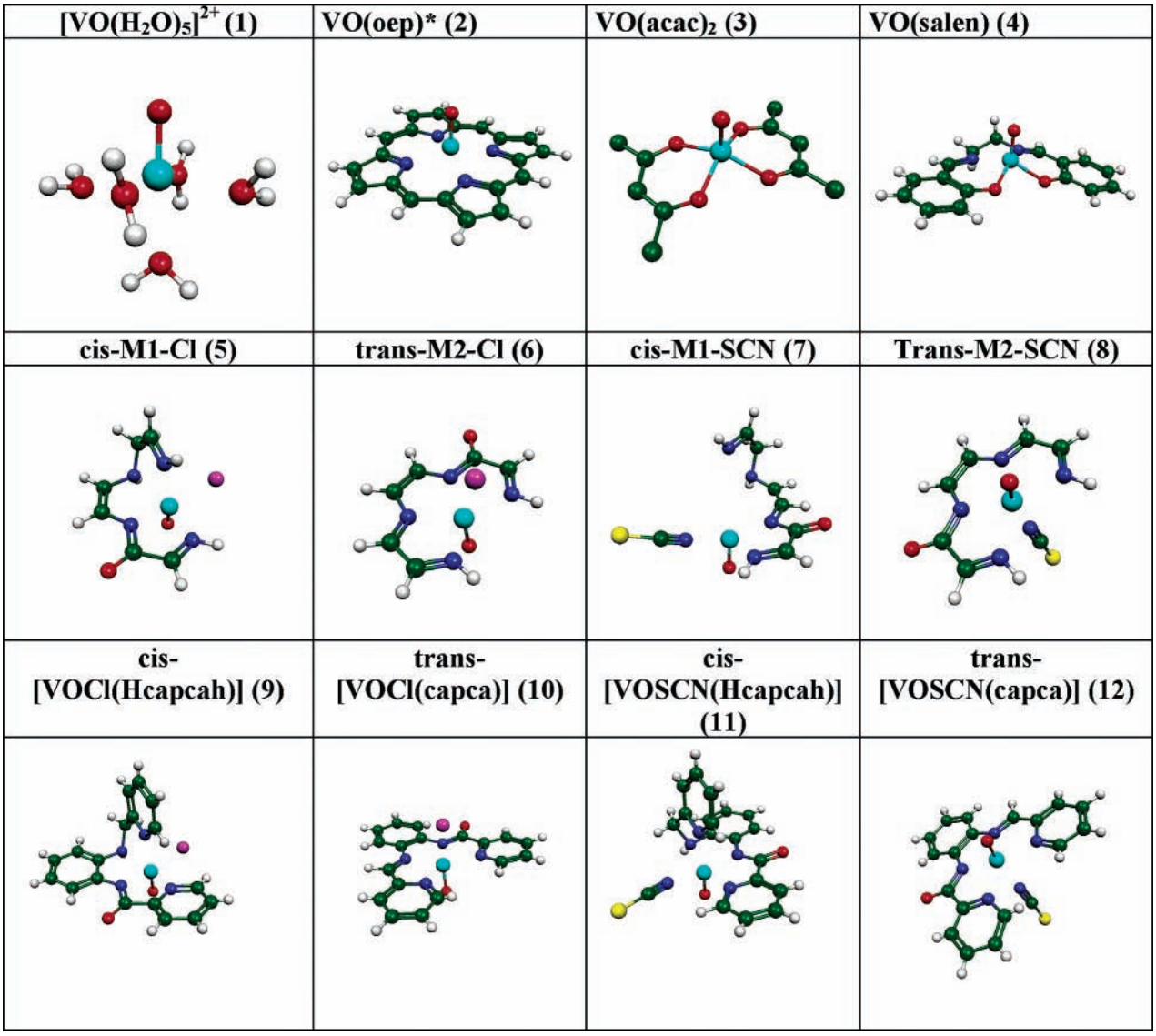

Figure 3. Geometries of the oxovanadium complexes used in the EFG and HF calculations optimized by DFT or extracted from the available crystral structures. In the structure from the X-ray crystal study of the VO(oep) complex, the ethylene fragments were replaced with protons.

(capca)] complexes reflect the presence of multiple species. These other species are most likely the cis isomers. ESE-detected spectra of the trans complexes are therefore simulated, which reflects this trans and cis equilibrium. The CW-EPR spectrum for *trans*-[VOCl(capca)] is simulated with 15% *cis*-[VOCl-(Hcapcah)] in the mixture, and the EPR spectrum of *trans*-[VOSCN(capca)] is simulated with 29% *cis*-[VOSCN-(Hcapcah)].

Figure 4 shows the ESE-ENDOR spectra obtained at the two applied magnetic fields corresponding to the $M_I = +^7/_2$ and $-^7/_2$ parallel turning points. At these fields, only molecular orientations with g_z approximately parallel to the applied magnetic field are sampled, providing spectra approximating those of a single crystal. Two split peaks, corresponding to the nuclear transitions in the α and β electron spin manifolds, are observed at each external magnetic field. Also, at the external magnetic field chosen in the experiment, the contribution of the cis species in *trans*-[VOC(capca)] complexes appears to be negligible.

Using a Fortran simulation program developed by Grant et al.,[18,36] the spectra in Figure 4 are simulated to determine the nqcc parameters. The simulation allows for the diagonalization of the full Hamiltonian matrix that includes the electronic Zeeman, nuclear Zeeman, and hyperfine and nuclear quadrupolar interactions. The parameters relevant to the simulation include the *g* tensor and hyperfine principal values that can be obtained by simulating the ESE-detected EPR or CW-EPR spectra. Other input parameters are experimental, such as the magnitudes of the external magnetic field and the microwave frequency. In addition, an initial estimate of the nqcc parameter is required. This can be obtained by using the equation derived by assuming the nuclear quadrupolar interaction to be a perturbation:[17,18,36]

$$\Delta\Delta\nu^{||}\left(\frac{7}{2}\right) = 2g_n\beta_n(B_{+7/2}B_{-7/2})24\mathbf{P}_{||} \qquad (6)$$

$\mathbf{P}_{||} = {}^3/_2P_{zz}$. P_{zz} is *z*th element, which is along the V=O bond, of nuclear quadrupolar tensor **P**. All nqcc values measured in this experiment are reported in terms of $\mathbf{P}_{||}$. $\Delta\Delta\nu^{||}(\pm^7/_2)$ represents the difference between the difference of the peaks at $M_I = {}^7/_2$ and $M_I = -^7/_2$. Estimates of the peak frequency were determined by fitting the experimental peaks with Gaussian curves. Simulated curves are shown by dotted lines in Figure 4. They are obtained by varying $\mathbf{P}_{||}$ until the best fit is obtained. Table 1 lists the $\mathbf{P}_{||}$ values. Best fits are obtained when $\mathbf{P}_{||}$ for *cis*-[VOCl(Hcapcah)] and *cis*-[VOSCN(Hcapcah)] are -0.35

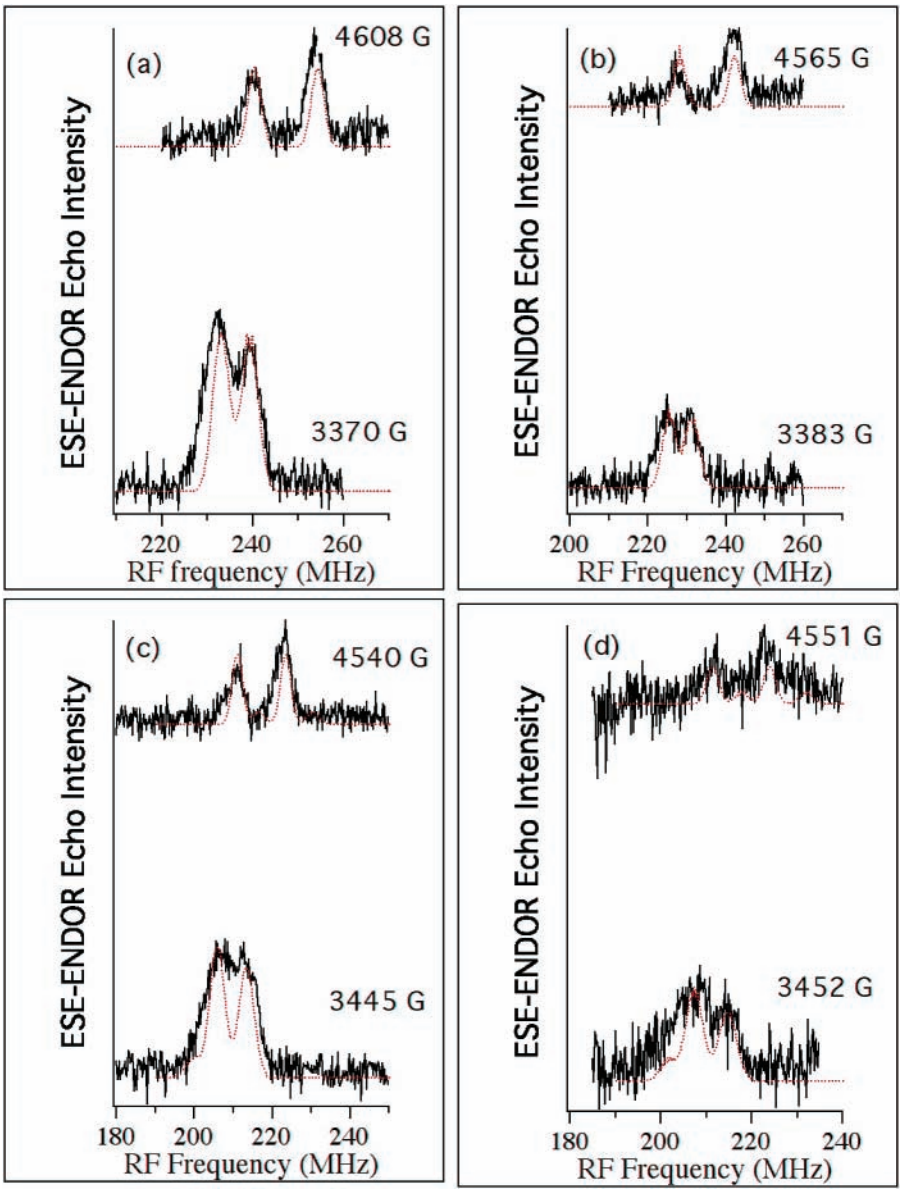

Figure 4. ^{51}V ESE-ENDOR spectra (—) for (a) *cis*-[VOCl(Hcapca)], (b) *cis*-[VOSCN(Hcapca)], (c) *trans*-[VOCl(capca)], and (d) *trans*-[VOSCN-(capca)]. Experimental parameters are (a) $\nu_{mw} = 10.8928$ GHz, $\tau = 500$ ns; (b) $\nu_{mw} = 10.8830$ GHz, $\tau = 520$ ns; (c) $\nu_{mw} = 10.8958$ GHz, $\tau = 300$ ns; and (d) $\nu_{mw} = 10.9250$ GHz, $\tau = 290$ ns. For a and b, $\pi/2 = 100$ and $\pi = 200$ ns in duration, whereas for c and d, $\pi/2 = 50$ and $\pi = 100$ ns. In all cases, the rf pulse width is 18 ms and $T = 20$ ms. For computer simulation (· · ·) by matrix diagonalization, $\mathbf{P}_{||}$ values are (a) −0.35 MHz, (b) −0.45 MHz, (c) −0.18 MHz, and (d) −0.21 MHz. The *g* and hyperfine principal values used are the same as in Figure 2. Simulations in panels c and d include 15% *cis*-[VOCl(Hcapcah)] and 29% *cis*-[VOSCN(Hcapcah)], respectively.

and −0.45 MHz, respectively. Using the same magnetic parameters used in the simulation of the *cis*-[VOX(Hcapcah)] and the fraction of cis species in the mixture, the best fits for the experimental ENDOR response for *trans*-[VOCl(capca)] and *trans*-[VOSCN(capca)] are obtained when $\mathbf{P}_{||}$ values are −0.18 and −0.21 MHz, respectively. In the simulation, the principal axes of *g*, *A*, and **P** were assumed to be coincident. Varying η has little or no effect on the overall simulation.

Discussion

The magnitude of the coupling constant depends on the intrinsic quadrupole moment of the nucleus and the electric field gradient at the nucleus. In the case of oxovanadium, the electric field gradient is established primarily along the V═O bond. It was previously demonstrated that $\mathbf{P}_{||}$ is greatly influenced by the presence of axial ligands but is insensitive to the variation of the donor ligands cis to the oxo bond.[17] Examples of vanadyl compounds with a vacancy in the axial position are VO(salen), VO(a cac)$_2$, and *N*,*N*-ethylenebis(*o*-*tert*-butyl-*p*-methylsalicylaldiminato) oxovanadium(IV). $\mathbf{P}_{||}$ for these complexes is estimated to be −0.9.[17,18,36] This value is large in magnitude in comparison to what we calculated for *trans*-[VOCl(capca)] (−0.18 MHz), *trans*-[VOSCN(capca)] (−0.21 MHz), *cis*-[VOCl(Hcapcah)] (−0.35 MHz), and *cis*-[VOSCN(Hcapcah)] (−0.45 MHz).

The substantial diminution in the magnitude of $\mathbf{P}_{||}$ indicates a decrease in the electric field gradient along the V═O bond. Ligands opposite the oxo bond donate electron density, thus counteracting the V═O bond. In other words, the pπ−dπ electron donation from oxygen to vanadium is reduced. Consequently, we can use the magnitude of $\mathbf{P}_{||}$ as an indicator of the V═O bond strength and the bond strength of ligands trans to the oxo bond. A small magnitude of $\mathbf{P}_{||}$ would indicate strong ligation at the site trans to the V═O bond and weakening of

TABLE 1: Experimental Values of $P_{||}$ for Various Oxovanadium Complexes Studied in This and in Our Previous Work and Compiled from the Available Litterature Data

VO complex	$\mathbf{P}_{\|}$ (MHz) from matrix diagonalization	$\mathbf{P}_{\|}$ (MHz) from perturbation theory	equatorial ligands	ref
trans-[VOCl(capca)]	−0.18	−0.09	N_4	this work
cis-[VOCl(Hcapcah)]	−0.35	−0.19	N_3Cl	this work
trans-[VOSCN(capca)]	−0.21	−0.12	N_4	this work
cis-[VOSCN(Hcapcah)]	−0.45	−0.28	N_4	this work
VO(salen)	−0.90	−0.43	N_2O_2	17, 36
VO(X-salen)[a]	−0.88	−0.43	N_2O_2	18
VO(salen)(pyridine)	−0.70	−0.37	N_2O_2	17, 36
VO(oep)	no data	−0.43	N_4	36
VO(oep)(imidazole)	no data	−0.40	N_4	36
VO(oep)(*n*-butyl amine)	no data	−0.24	N_4	36
$VO(acac)_2$	−0.90	−0.43	O_4	17, 36
$VO(acac)_2$(EtOH)	−0.50	−0.25	O_4	17, 36
$VO(acac)_2$(DMSO)	no data	−0.22	O_4	36
$VO(acac)_2$(pyridine)	no data	−0.10	O_3N	36
$[VO(H_2O)_5]^{2+}$	−0.20	−0.13	O_4	17

[a] X-salen = *N*,*N*′-ethylenebis(*o*-tertbutyl-*p*-methylsalicylaldiminato).

the V═O bond. The IR V═O stretching frequency of oxovanadium compounds has been correlated to the strength of the V═O bond.[40,41] Oxovanadium compounds have characteristic V═O stretching frequencies at around 960 ± 50 cm^{-1}.[42] A previous IR study[41] has shown a decrease in the V═O stretching frequencies of pyridine and substituted pyridine adducts of $VO(acac)_2$, suggesting that pyridine binds cis to the oxo bond by displacing one of the acetylacetonato ligands and allowing the displaced ligand to bind trans to the oxo group. A recent ^{51}V ESE-ENDOR study corroborates this result.[17] Analogously, we should expect *trans*-[VOCl(capca)] and *trans*-[VOSCN(capca)] to have strong bonding at the axial site, resulting in the weakening of the V═O bond, which evident in the lowering of their V═O stretching frequency.[12]

Table 1 provides a short compilation of $\mathbf{P}_{||}$ values calculated by the matrix diagonalization procedure and perturbation theory using data obtained from pulsed ENDOR studies of some vanadyl compounds. One interesting observation is that *trans*-[VOCl(capca)] and *trans*-[VOSCN(capca)] have smaller $\mathbf{P}_{||}$ values than those complexes with neutral axial ligands. It appears that charged ligands, bound axially, are more effective than the neutral ligands in donating electrons to the metal center, even contradicting the order in the traditional spectrochemical series. A similar trend was observed in the experiment done by Ashby et al.[43] in which the effect of charged ligands on the donor orbital occupancy of the imino nitrogen of imidazole ligated to a Lewis acid was determined. The contribution of these charged ligands can be quantitatively determined using the expression

$$V_{zz} = eq_{zz} = -\frac{e(3\cos^2\theta - 1)}{r^3} \qquad (7)$$

r in the above equation is the distance from the nucleus to the electric field gradient source. In earlier work, anionic ligands were found to reduce A_z by up to 16% with respect to A_z values of complexes with similar ligand donor sets. *Trans*-[VOCl(capca)] and *trans*-[VOSCN(capca)] have A_z values of 435 and 440 MHz, respectively. The corresponding *cis*-[VOCl(Hcapcah)] and *cis*-[VOSCN(Hcapcah)] have A_z = 495 and 471 MHz, respectively. Whereas the A_z values for these cis compounds are more or less typical of what is expected according to the equatorial donor atom, the A_z values of the trans compounds deviate from the g_z versus A_z correlation plot. (See the A_z versus g_z correlation plot in Figure 4 of ref 12.) Thus the A_z value changes only when a charged axial ligand is present. Otherwise stated, the A_z value cannot discern the existence of a neutral axial ligand. Our ENDOR experiment, however, indicates that $\mathbf{P}_{||}$ is a sensitive parameter for probing axial ligation as we observed that $\mathbf{P}_{||}$ (charged axial ligand) < $\mathbf{P}_{||}$ (neutral axial ligand) < $\mathbf{P}_{||}$ (vacant axial position).

Tolis et al.[12] provided an explanation as to why the hyperfine value A_z is reduced upon the ligation of charged ligands. Negatively charged ligands were assumed to induce the radial expansion of the $3d_{xy}$ orbital, where the unpaired electron mostly resides. The expansion of this orbital implies that the dipolar interaction, $\mathbf{P} = g_n\beta_n g_e\beta_e\langle r^{-3}\rangle$, between the vanadyl nucleus and the unpaired electron is reduced. The same reasoning could be applied to explain why negatively charged axial ligands provide small $\mathbf{P}_{||}$ values as V_{zz} is inversely dependent on $\sqrt[3]{r}$. Thus, we observed a small $\mathbf{P}_{||}$ for *trans*-[VOCl(capca)] and *trans*-[VOSCN(capca)]. In addition to the effect of the charged axial ligands on $\mathbf{P}_{||}$, the geometry assumed by VO complexes, as ligands are added, plays an important role as shown recently by ESE-ENDOR results reported by Grant et al.[18] For a series of pentacoordinated oxovanadium compounds, $\mathbf{P}_{||}$ decreases as the geometry changes from square pyramidal to distorted trigonal bypyramidal. Therefore, in determining the contribution of axial ligands to the nqcc of vanadium, the geometry of the resulting complex, electron-donating tendency, and charge of the ligands have to be considered.

Calculated Quadrupolar Parameters. The results of the calculations of the quadrupolar coupling constant C_q for aqua VO complex $[VO(H_2O)_5]^{2+}$ with various basis sets are presented in Table 2 and plotted in Figure 5a. These data clearly show that the use of small basis sets, such as 3-21g*, is inaccurate. But even with computationally expensive basis sets such as 6-311++g or 6-311++g**, the desired accuracy cannot be achieved. Surprisingly, the augmentation of the basis set with polarization functions (6-311++g** versus 6-311++g) has only a very slight impact on the resulting C_q value.

To determine if this trend is intrinsic to the particular molecule or if it a general tendency of the oxovanadium(IV) complexes, we have repeated the same set of calculations on the *cis*-[VOCl(Hcapcah)] and *trans*-[VOCl(capca)] complexes with structures based on the coordinates extracted from the crystal structures of these compounds (Figure 5). Whereas in the case of the *cis*-[VOCl(Hcapcah)] compounds the 3-21g* basis set seems to give the result closest to the experimental value, it is clear that the calculated value for the trans complex again shows the inac-

TABLE 2: Calculated and Experimental Values of C_q for $[VO(H_2O)_5]^{2+}$ Computed with Different Basis Sets at the B3LYP Level (Gaussian 98) as Well as with the SR UKS and SO + SR ROKS Methods (Basis Set TZ2P) with BP86 and BLYP Functionals (ADF 2002)[a]

$[VO(H_2O)_5]^{2+}$	3-21g*	6-31g*	TZV	6-311++g	6-311++g**	exptl
V_{xx}	0.087	−0.129	−0.105	−0.101	−0.068	
V_{yy}	0.171	−0.206	−0.190	−0.202	−0.191	
V_{zz}	−0.259	0.335	0.294	0.303	0.260	
C_q	−3.18	4.12	3.63	3.73	3.20	5.60

	SR UKS/BP86	SR UKS/BLYP	SO+SR ROKS/BP86	SO+SR ROKS/BLYP
C_q	4.35	4.51	4.67	4.81

[a] See ref 29 for details.

TABLE 3: DFT-Calculated Values of $P_{||}$ (MHz) for the Oxovanadium Complexes Studied in This and in Our Previous Work[a]

	trans-[VOCl (capca)]	*cis*-[VOCl (Hcapcah)]	*trans*-[VOSCN (capca)]	*cis*-[VOSCN (Hcapcah)]	VO(oep)	$VO(acac)_2$	VO(salen)
V_{xx}	0.019	−0.075	0.079	−0.134	0.386	−0.090	0.389
V_{yy}	0.162	−0.257	0.127	−0.391	0.415	−0.212	0.497
V_{zz}	−0.182	0.332	−0.277	0.526	−0.802	0.302	−0.886
$\mathbf{P}_{||}$	0.08	−0.15	0.12	−0.23	0.35	−0.14	0.38
exptl	−0.18	−0.36	−0.21	−0.45	−0.43	−0.43	−0.43

[a] Calculations were performed at the B3LYP level with the 6-311++g basis set.

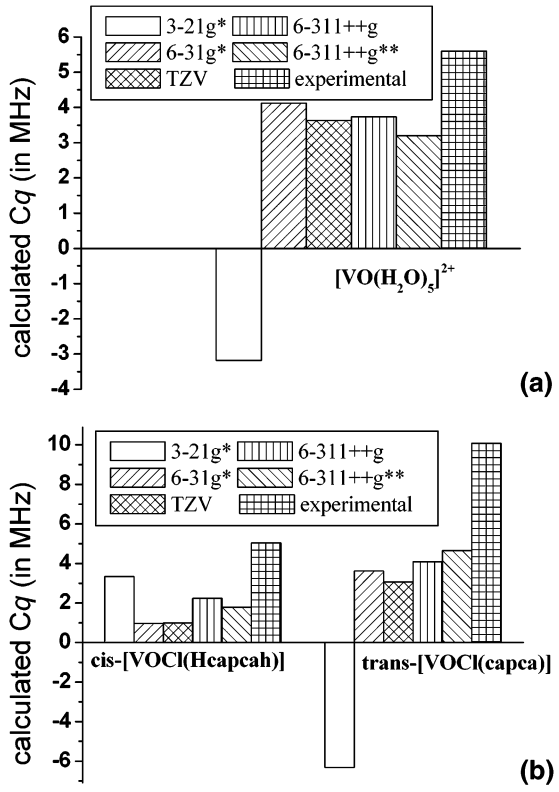

Figure 5. Comparison of C_q values of oxovanadium complexes calculated by DFT using various basis sets. The complexes used for the calculations are (a) $[VO(H_2O)_5]^{2+}$ and (b) *cis*-[VOCl(Hcapcah)] and *trans*-[VOCl(capca)].

curacy of this basis set, indicating to us that the result for the cis complex is a coincidence. By analyzing both series of results together with the calculated EPR hyperfine tensors (see the next section), a choice of the triple-ζ 6−311 g++ basis set of Pople and co-workers with diffused functions seemed to us to be a good compromise between the expense of the computational time and the desired accuracy, and thus this basis set was used for further calculations. For the sake of comparison, an additional set of calculations on the vanadium pentaqua complex (**1**) was performed with the ADF program using a relativistic ZORA Hamiltonian, which includes scalar relativistic (SR) and

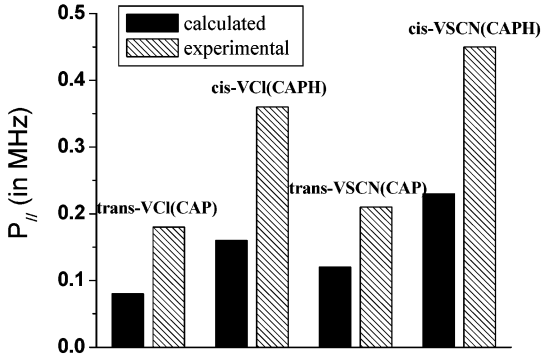

Figure 6. Bar plot comparing the calculated and experimental C_q values for *cis*-[VOCl(Hcapca)], *cis*-[VOSCN(Hcapca)], *trans*-[VOCl(capca)], and*trans*-[VOSCN(capca)]. A triple-ζ 6-311++g basis was used for the calculations.

spin−orbit (SO) coupling. Two approaches were used: the SR spin-unrestricted open-shell Kohn−Sham (SR UKS) and the SO coupling and SR spin-restricted open-shell Kohn−Sham (SO + SR ROKS); for details, see ref 29. The obtained C_q values are relatively close to those calculated with the nonrelativistic approach (Table 2). However, better agreement with the experimental value is obtained with the SO + SR ROKS approach combined with the BLYP functional.

The computed and experimental values of $\mathbf{P}_{||}$ for the cis and trans complexes studied by ESE-ENDOR are presented in Figure 6. Whereas the absolute values of $\mathbf{P}_{||}$ cannot be reproduced with sufficient accuracy, even using a computationally expensive, large basis set, the qualitative agreement with the experimentally observed trends is very satisfactory. Consistent with the experimental evidence, the modification of the geometry of the oxovanadium complex from the trans to the cis form (which results in a change in the presence of a negatively charged ion from the axial to the equatorial position, respectively) causes a net increase of the calculated values of $\mathbf{P}_{||}$. Moreover, the relative difference between the trans and cis forms (about 100% of the absolute experimental values of $\mathbf{P}_{||}$) is well reproduced by DFT calculations.

In the second part of this study, we have also calculated $\mathbf{P}_{||}$ values for three oxovanadium complexes previously studied in our laboratory. These results are compiled with the complexes studied in this work in Table 3. In the case of $VO(acac)_2$, the

TABLE 4: Calculated Values of C_q (MHz) for Model Complexes M1 and M2 with Cl^- and SCN^- Ions[a]

	cis-M1−Cl	*trans*-M2−Cl	*cis*-M1−SCN	*trans*-M2−SCN
V_{xx}	−0.128	0.001	−0.338	−0.069
V_{yy}	−0.204	−0.154	−0.411	−0.379
V_{zz}	0.331	0.155	0.750	0.448
C_q	4.08	1.90	9.23	5.52

[a] Calculations were performed at the B3LYP level with the 6-311++g basis set.

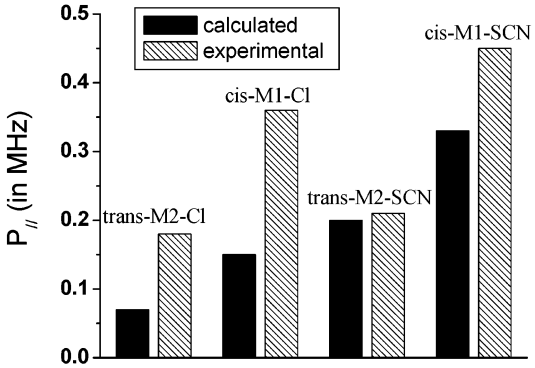

Figure 7. Plot of C_q values of the optimized model complexes of *cis*-M1−Cl (**5**), *trans*-M2−Cl (**6**), *cis*-M1−SCN (**7**), and *trans*-M2−SCN (**8**). Calculations were performed at the B3LYP level with the 6-311++g basis set. Also plotted are the experimentally determined C_q values of *cis*-[VOCl(Hcapca)], *cis*-[VOSCN(Hcapca)], *trans*-[VOCl-(capca)], and *trans*-[VOSCN(capca)].

calculated $\mathbf{P}_{||}$ is smaller than the experimental value, in agreement with the trend observed in the previous series of calculations. Surprisingly, in the case of porphyrin complexes VO(oep) and VO(salen), the calculated $\mathbf{P}_{||}$ values are close to the experimentally detected couplings. This can be somehow related to two facts that must be mentioned here. Primarily, both species are highly symmetrical and rigid, which suggests that the inputed geometries are close to the experimental conformation, which is in contrast to the $VO(acac)_2$ complex, which has an additional degree of freedom and whose geometry can be distorted in the liquid or frozen solution. The second concerns the fact that these three complexes are free and that the electric field at the vanadium nucleus is essentially dictated by the symmetrical O-axial−N(O)-equatorial environment and it is not perturbed by the surrounding charged ions, as in the case of the vanadium capca and capcah complexes or by the presence of the oxygen in the axial position in the case of $[VO(H_2O)_5]^{2+}$.

Keeping in mind the usefulness of the simplified models that mimic complicated systems in quantum chemical calculations in order to reduce computational expenses, we have also computed the values of C_q for four model molecules with minimum features mimicking the real cis and trans oxovanadium complexes (**9**−**12**). The calculated values of C_q (Table 4) indicate that this simple model only partially satisfies the required criteria. In the cases of *cis*-M1−Cl, *trans*-M2−Cl, and *cis*-M1−SCN, the calculated values of C_q are almost identical to those calculated from the crystal structure of *cis*-[VOCl(H capcah)], *trans*-[VOCl(capca)], and *cis*-[VOSCN(Hcapcah)], respectively (Figure 7). However, in the case of the *trans*-M2-SCN model compound, the calculated value is very close to the experimental value and clearly diverges from the previously observed trend.

A careful analysis of the geometrical features of the optimized structure of *trans*-M2−SCN indicates that in the case of the cis isomer the optimized structure of the model molecule almost exactly reproduces the primary coordination sphere of vanadium as determined from the X-ray crystal study. This situation is different in the case of the trans isomer. To the best of our knowledge, the crystal structure of *trans*-[VOSCN(capca)] has not been published; therefore, we could not perform the calculations on this molecule using coordinates extracted from an X-ray structure. The optimized V═O distances in the *trans*-[VOSCN(capca)] and *trans*-M2−SCN molecules are the same (1.63 Å), but the optimized V−Cl distance is noticeably longer in the model compound (2.57 versus 2.26 Å) than in *trans*-[VOSCN(capca)]). By performing a series of simple calculations on the hypothetical $O{=}V{-}Cl^+$ molecule with different V−Cl distances, we found that the electric field gradient is very sensitive to the distance of the vanadium nucleus from the axial, negatively charged substituent. This is not surprising because the electric field on the vanadium atom is directly perturbed by the proximity of the charged axial ion. Therefore, a slight difference in the V−Cl distance is directly reflected by the important change in the calculated value of C_q. We are currently investigating the influence of the geometrical conformation of the counterion (distance, axial or equatorial position) on the calculated EFG of the vanadium nucleus.

It should be mentioned that the choice of the right geometry for the computation of the EFG of the paramagnetic vanadium complexes is the crucial point in the mentioned methodology. Almost all of the solid-state NMR studies on the diamagnetic compounds were performed in single crystals, ensuring that the geometry used for the computation of the C_q values is almost identical to those present under experimental conditions. However, this is not the case for paramagnetic V(IV) complexes; the majority of the EPR and ESE-ENDOR studies are performed in liquid or frozen solutions. Therefore, the geometries used for the computation of the EFG could be slightly different from those present under experimental conditions. Sometimes the QM geometry optimization, including, for example, solvent effects, can help in determining the "right" input geometry, but in almost all cases, a difference between the optimized and real experimental geometry can be a source of substantial errors in the calculated values of the EFG.

In the context of the calculations of the NQR interactions, it is interesting to compare our results to the previous theoretical studies on the quadrupolar parameters in diamagnetic molecules. The values of C_q calculated for some organic complexes of V(V), together with similar calculations for Zn complexes,[44] are presented in Figure 8a and b. In the case of the diamagnetic oxovanadium compounds, there is almost perfect agreement between the calculated and experimental values of the quadrupolar coupling constant for two complexes; the calculated values for two other complexes are overestimated by about 25%. More surprisingly, in the case of heavier elements such as Zn, the nonrelativistic calculations with a rather small basis set (6-31g-(f)) are in good agreement with the experimental values (except for the complex with urea acetate) even if one expects small relativistic and correlation effects for zinc in Zn(II) coordination complexes. To check the validity of our calculations, we have recalculated the C_q values for these latter complexes and have obtained the same results as in ref 44. Thus, it appears that the EFG calculations for the diamagnetic species yield results that are substantially closer to the experimental values than calculations for the paramagnetic complexes such as those studied in this work.

Calculated Hyperfine Coupling Constants. In this part of our theoretical investigation, we have applied similar methodology to calculations of the isotropic and anisotropic parts of the ^{51}V hyperfine interaction. The results of the calculations of the

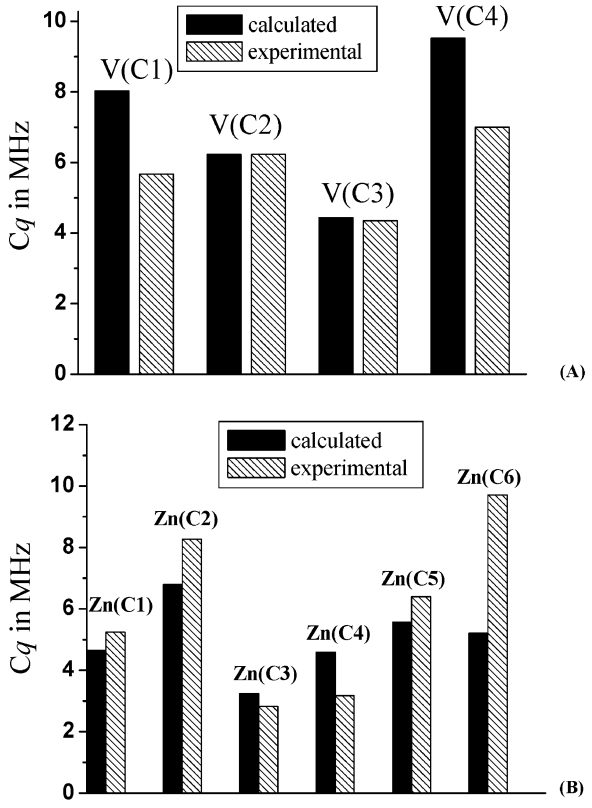

Figure 8. Comparison of calculated and experimental values of C_q for some organic diamagnetic complexes of (A) vanadium and (B) zinc. ^{51}V calculations were performed at the B3LYP level with the 6-311++g basis set. ^{65}Zn calculations were performed at the B3LYP level with the 6-31g* basis set. (A) V(C1) = (oxa)bis[oxobis(8-quinolinolato)-vanadium(V)], V(C2) = oxoperoxo(pyridine-2,6-dicarboxylato)vanadate(V) hydrate, V(C3) = [VO(OEt)(salicyl aldehyde[benzylmercaptothiocarbonylhydrazonate])], V(C4) = VO_2[Acpy-iNH]. For detailed molecular structures, see ref 30 and references therein. (B) Zn(C1) = Zn(acetate)$_2$·2H$_2$O, Zn(C2) = Zn(imidazole)$_2$(acetate)$_2$, Zn(C3) = Zn(imidazole)$_4$(ClO_4)$_2$, Zn(C4) = Zn(thiourea)$_4$(NO_3)$_2$, Zn(C5) = Zn(formate)(acetate)$_2$ − site 1, Zn(C5) = Zn(formate)(acetate)$_2$ − site 2. For detailed molecular structures, see ref 44 and references therein.

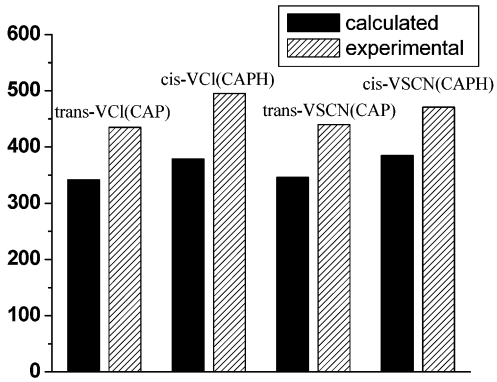

Figure 9. Plot comparing the DFT-calculated and experimentally determined A_{zz} values for cis and trans vanadyl compounds. Calculations were performed at the B3LYP level with the 6-311++g basis set.

hyperfine tensors for the four oxovanadium complexes studied in this work are presented in Figure 9. As in the case of the calculations of the quadrupolar interactions, the experimentally observed trends are nicely reproduced by the calculations, but the calculated absolute values of the HF tensor elements show a statistical error of about 100 MHz between the experimental and calculated values of A_{zz}. This is expected because it is well

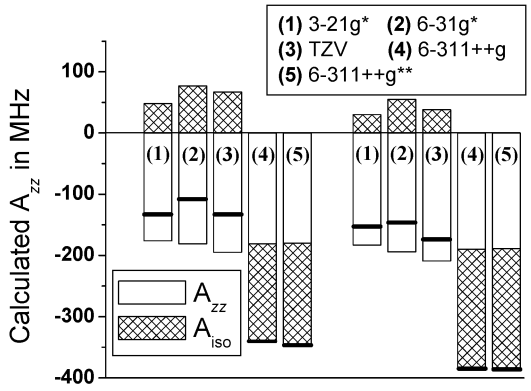

Figure 10. Parallel hyperfine tensor element for *cis*-[VOCl(Hcapcah)] and *trans*-[VOCl(capca)] calculated with DFT using various basis sets. The bold black lines indicate the calculated absolute value of A_{zz}, and the dashed and white bars show the participation of the isotropic and anisotropic parts of the computed hyperfine tensor element.

known that the agreement between experimental and DFT-calculated values of the isotropic Fermi contact is only modest.[45] To visualize this effect, in Figure 10 we have represented the values of A_{zz} for *cis*-[VOCl(Hcapcah)] and *trans*-[VOCl(capca)] calculated with various basis sets (Table 5). It is straightforward to notice that the dipolar part of the hyperfine interaction is calculated with the same accuracy almost independently of the basis set, whereas the isotropic Fermi contact term is completely inaccurate with the 3-21g*, 6-31g*, and triple-ζ TZV basis sets. Only by introducing the extended basis sets (6-311++g or 6-311++g**) can the isotropic part be computed with reasonable accuracy, but even the use of such basis sets gives unsatisfactory results. Recently, Saladino and Larsen[29] calculated the anisotropic and isotropic parts of the hyperfine coupling constant for vanadium in the oxovanadium complex [VO(imid)-$(H_2O)_4]^{2+}$ with the zeroth-order regular approximation (ZORA) that includes the relativistic effects as implemented in the Amsterdam density functional (ADF) package. It appears that a net improvement in the calculated values of the vanadium isotropic Fermi contact can be obtained by using the scalar-relativistic, spin-unrestricted, open-shell Kohn−Sham (SR UKS) calculations. Another article by Saladino and Larsen,[46] following the recent advances in the computation of the HF tensors by Munzarova and Kaupp,[47,48] suggests that better agreement of the isotropic hyperfine constant A_{iso} with the experimental data is obtained when half-and-half hybrid functionals are used for the DFT calculations. Therefore, we have also recalculated the HF tensors using the half-and-half functional BHandHLYP[49] as implemented in Gaussian 98. The results of these calculations are reported in Table 6. The calculated A_{iso} values are in much better agreement with the experimental data, confirming that the use of the hybrid half-and-half functionals is more appropriate for the calculations of the Fermi contact values in this class of vanadium compounds. The calculated values of the dipolar part of the hyperfine tensors are almost unaffected; therefore, we conclude that they are less sensitive to the functionals used.

Some interesting comments might be made about the relation between the geometry of the investigated complexes and the spatial shape of the hyperfine tensor obtained from the DFT calculations. As can be seen from Table 6 (and as schematically visualized in Figure 11), the hyperfine tensor has perfectly axial symmetry in the case of both cis complexes. In the case of the trans complexes, however, this tensor shows a net deviation from axial symmetry, which is translated into a difference between the two smaller tensor elements of about 60 MHz. As expected, the direction of A_{zz} in all of the complexes coincides

TABLE 5: DFT-Calculated Values of A_{zz} (MHz) for Two Oxovanadium Complexes Studied in this Work, *cis*-[VOCl(Hcapcah)] (9) and *trans*-[VOCl(capca)] (10), with Different Basis Sets[a]

	3-21g*	6-31g*	TZV	6-311++g	6-311++g**	6-311++g	exptl
(**9**)						*cis*-M1−Cl (**5**)	
A_{iso}	48	77	67	−161	−168	−171	
t_1	58	52	60	58	59	60	
t_2	118	128	135	123	122	122	
t_3	−176	−181	−195	−181	−180	−181	
A_{xx}	106	129	127	−38	−46	−49	
A_{yy}	166	205	202	−103	−109	−111	
A_{zz}	−128	−104	−128	−342	−348	−352	−435
(**10**)						*trans*-M2−Cl (**6**)	
Aiso	30	55	38	−196	−198	−198	
t_1	87	90	96	92	92	92	
t_2	96	103	114	98	98	98	
t_3	−183	−194	−209	−190	−189	−191	
A_{xx}	117	145	134	−98	−100	−100	
A_{yy}	126	158	152	−104	−106	−106	
A_{zz}	−153	−139	−171	−386	−387	−389	−495

[a] For the sake of comparison, the calculations on model compounds *cis*-M1−Cl (**5**) and *trans*-M2−Cl (**6**) with the 6-311++g basis set are also reported.

TABLE 6: DFT-Calculated and Experimental Values of A_{xx}, A_{yy}, and A_{zz} (MHz) for the Four Oxovanadium Complexes Studied in this Work[a]

	cis-[VOCl (Hcapcah)] (**9**)	*trans*-[VOCl (capca)] (**10**)	*cis*-[VOSCN (Hcapcah)] (**11**)	*trans*-[VOSCN (capca)] (**12**)
		B3LYP functional		
A_{iso}	−196	−161	−197	−163
t_1	92	58	91	61
t_2	98	123	97	122
t_3	−190	−181	−188	−183
A_{xx}	−98	−38	−100	−41
A_{yy}	−104	−103	−106	−102
A_{zz}	−386	−342	−385	−346
		BHandHLYP functional		
A_{iso}	−256	−231	−258	−230
t_1	96	69	96	70
t_2	102	122	103	122
t_3	−198	−191	−199	−193
A_{xx}	−160	−162	−162	−160
A_{yy}	−154	−109	−155	−108
A_{zz}	−454	−422	−457	−423
		experimental		
A_{iso}	−279	−246	−263	−246
A_{xx}	−172	−157	−160	−156
A_{yy}	−170	−145	−160	−144
A_{zz}	−495	−435	−471	−439

[a] Calculations were performed using the B3LYP and half-and-half BHandHLYP functionals with the 6-311++g basis set.

with the V═O bond, but interestingly, the direction of the larger perpendicular HF tensor element in the trans complexes lies in the asymmetric plane. This plane is a bisector of four nitrogen atoms along the V═O bond. Thus, in the trans complexes the HF tensor is "compressed" in the direction coinciding with the pseudo-2c_v axis of the capca ligand. When a negatively charged atom is present on this latter axis (and this is obviously the case for the cis complexes), the interaction of the negative ion with the molecular orbital containing single electron affects the spatial shape of the orbital, generating an "elongation" in this direction. This results in almost perfect axial symmetry of the HF tensor. However, this deviation from axiality is not observed in the experimentally obtained data. Comparing the experimental values of the perpendicular HF tensor elements to those obtained from the DFT calculations, it is straightforward to notice that the obtained experimental values deviate only slightly from perfect axial symmetry ($\Delta_{A_{xx}-A_{yy}} = 12$ MHz for trans complexes **10** and **12**; $\Delta_{A_{xx}-A_{yy}} = 2$ and 0 MHz for cis complexes **9** and **11**, respectively). The simulations of the experimental spectra with the QPOW program using the DFT-calculated values of the dipolar part of the HF tensor (including the experimentally obtained A_{iso}) result in the simulated spectra, which differ significantly from the experimental lines. Therefore, we conclude that the axial experimental values of the HF tensors might

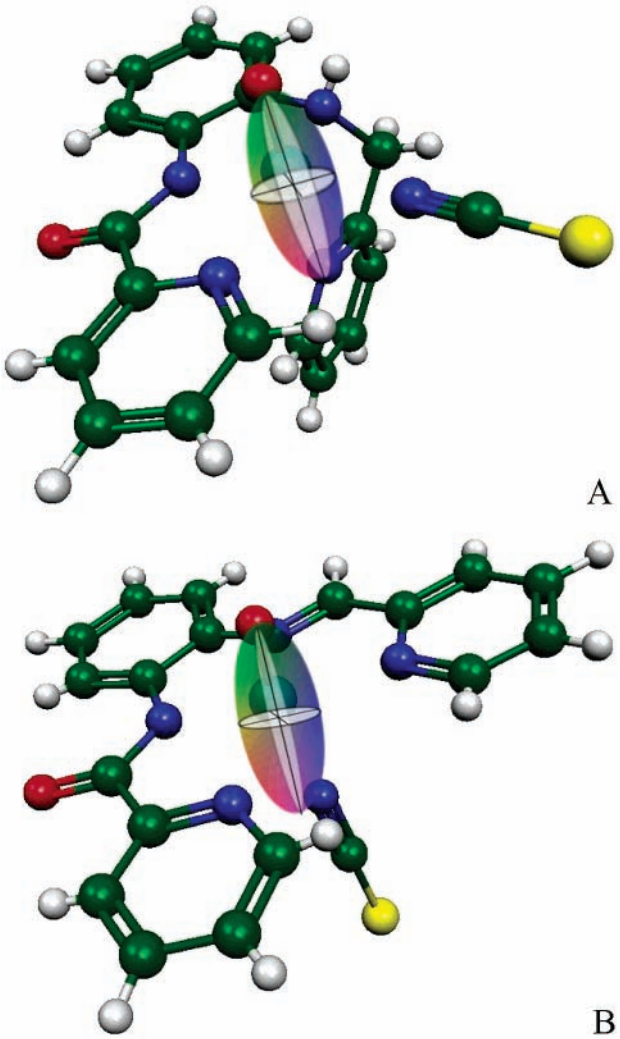

Figure 11. Spatial representation of the hyperfine tensor calculated with DFT for *cis*-[VOSCN(Hcapcah)] and *trans*-[VOSCN(capca)].

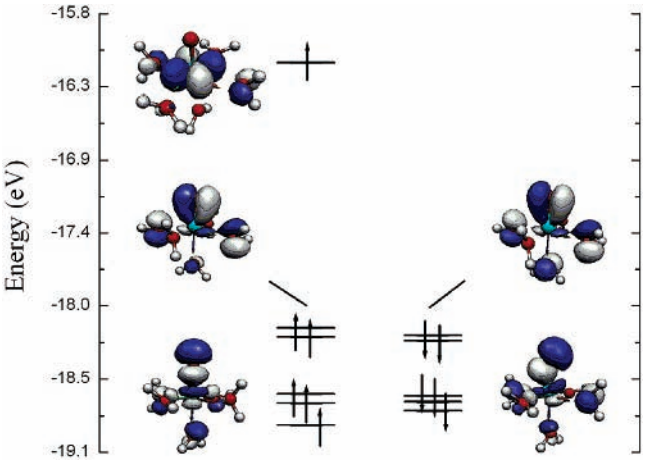

Figure 12. Schematic energy-level diagram for Kohn−Sham frontier orbitals of $[VO(H_2O)_5]^{2+}$ in the ground state obtained from spin-unrestricted DFT calculations.

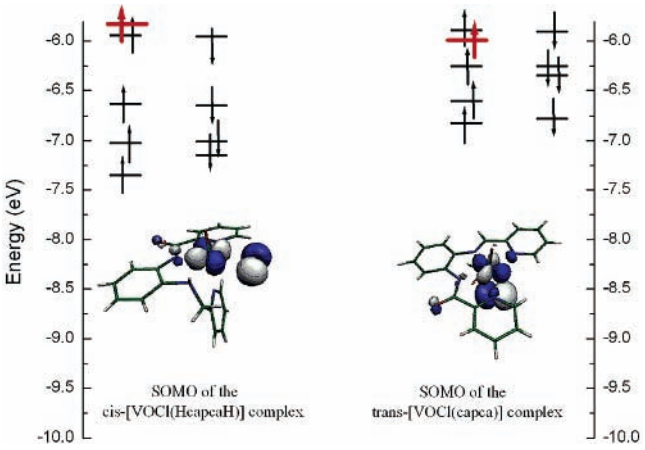

Figure 13. Schematic energy-level diagram for Kohn−Sham frontier orbitals of *cis*-[VOCl(Hcapcah)] and *trans*-[VOCl (capca)] in the ground state obtained from spin-unrestricted DFT calculations.

be affected by the solvent or conformational effects that are not reproduced by our DFT calculations. Finally, it is also worth noting that the difference in the experimental A_{zz} values between cis and trans complexes ($\Delta A_{zz} = 60$ MHz for complexes with Cl^- and 31 MHz for complexes with SCN^- ion) is also reflected by the B3LYP calculations ($\Delta A_{zz\ calcd} = 44$ and 39 MHz, respectively). But interestingly, whereas the calculated ΔA_{iso} between the cis and trans species is almost identical for both types of complexes ($\Delta A_{iso\ calcd} = 35$ MHz for Cl^- and 34 MHz for SCN^- complexes), the computed difference in the total spin density from Mulliken analysis on the vanadium atom at the B3LYP level is quite different: $\Delta_{spin} = 0.008$ for Cl^- and $\Delta_{spin} = 0.098$ for SCN^- complexes.[50]

Electronic Structure and Molecular Orbitals. In the context of this work, we also found it interesting to explore the information about the electronic structure of the studied compounds that might be extracted from our DFT calculations. First, we will consider the case of the $[VO(H_2O)_5]^{2+}$ complex, whose electronic structure was predicted some time ago.

The optimized structure of the aqua vanadyl ion is slightly distorted (Figure 3). For the sake of simplicity, for the discussion of the molecular orbitals obtained from DFT calculations we will consider only the vanadyl ion with an axial oxygen, surrounded symmetrically by five oxygens from water molecules; this environment would correspond to C_{4v} symmetry. Within the assumption of this symmetry, the orbital containing a single unpaired electron (Figure 12) is close to b_2 symmetry; the calculated MO indicates that this is not a pure $3d_{xy}$ orbital as in the case of the VO^{2+} ion but rather a hybrid orbital with some admixture of metal $3d_{x^2y^2}$ and $2p_y$ orbitals from two neighboring oxygens (Figure 12). The next occupied MOs (which are about 2.2 eV lower in energy) are occupied by 2α and 2β electrons in hybrid π orbitals that are essentially composed of vanadium $3d_{yz}$ and $3d_{xz}$ orbitals and $2p_y$ and $2p_x$ orbitals of the axial oxygen, with some additional $2p_y$ and $2p_z$ character from two neighboring water oxygens. The next four electrons are confined in the hybrid s-type orbital with metal contributions from $3d_{z^2}$, $3p_z$, and 3s orbitals and from the $2p_z$ orbital of the axial oxygen. In this case, a small contribution from $2p_y$ and $2p_z$ from two neighboring water oxygens is present. This picture of frontier molecular orbitals is consistent with MOs and the bonding scheme proposed by Ballhausen and Gray.[51]

The most interesting feature of the molecular orbitals of oxovanadium complexes is the MO containing the single electron. As an example to illustrate the influence of the position of the negatively charged ion on the calculated hyperfine and quadrupolar parameters, we have chosen the two complexes with the Cl^- ion, but the same conclusions apply to the two other complexes with the isocyanate ion. Figure 13 shows the SOMO orbitals of *cis*-[VOCl(Hcapcah)] and *trans*-[VOCl(capca)]. Although it is generally agreed that in the oxovanadium(IV) complexes the SOMO containing the single unpaired electron is principally a $3d_{xy}$ orbital of the vanadium, in the case of the presence of the negatively charged counterion there is a net interaction with this negatively charged nucleus. To understand the principal effect affecting the spin distribution on the vanadium nucleus (and thus the value of A_{zz}) as well as the electric field gradient, we have compared the picture of frontier orbitals and have carefully examined the charge and spin distributions in both molecules. As already outlined in the EPR section, the transition of the counterion from cis to trans geometry seems to affect the spin distribution of the $3d_{xy}$ orbital of vanadium by the spatial modification of the orbital shape, which is most likely related to the spatial expansion of the electronic cloud, reducing the observed A_{zz} values. The analysis of the calculated MO coefficients shows that the SOMO orbital for both complexes is a mixture of $3d_{xy}$ and $3d_{x^2y^2}$ orbitals. Indeed, in the case of the cis complex, d_{xy} character is predominant, whereas a contrary effect is observed in the case of the trans complex. This is in agreement with the previously observed ground-state electronic structures of vanadium complexes.[20] The electron is mainly confined in the $3d_{xy}$ function for C_{4v} symmetry and in the $3d_{x^2y^2}$ function for C_{2v} symmetry. In the case of distorted "average" symmetry, a single electron resides in the degenerate $3d_{xy}$ and $3d_{x^2y^2}$ orbitals. We have also investigated the possibility that because of the interaction with the negatively charged counterion some $3d_{z^2}$ character will appear in the SOMO orbital containing the single electron. In the calculated MO, the contribution of $3d_{z^2}$ character to the SOMO orbitals in both complexes is insignificant, and thus we conclude that the contribution of the $3d_{z^2}$ orbital to the SOMO cannot be considered to be a possible mechanism for the reduction of A_{zz} values in trans complexes.

Conclusions

The results of this work demonstrate the versatility of ESE-ENDOR in measuring both metal-center nuclear spin transitions and the effects of axial ligand interactions that are weak and unresolved by CW-EPR spectroscopy. We were able to measure

the nuclear coupling constant of ^{51}V for four oxovanadium compounds by applying the technique of ESE-ENDOR. Negatively charged ligands binding trans to the oxo bond were found to have smaller nqcc values than those of neutral ligands binding trans to the oxo bond. In general, we observed that $\mathbf{P}_{||}$ (charged axial ligand) < $\mathbf{P}_{||}$ (neutral axial ligand) < $\mathbf{P}_{||}$ (vacant axial position). In combination with CW-EPR, this finding suggest that we may be able to distinguish the identity of the ligand coordinating trans or cis to the oxo bond by pulsed-ENDOR. The complementary use of quantum mechanical calculations shows that DFT theory is able to predict experimentally observed trends for the changes in the quadrupolar and hyperfine parameters of paramagnetic oxovanadium complexes upon the configurational changes in the geometry of the neighboring negatively charged counterion. Unfortunately, the desired accuracy in the calculation of the isotropic Fermi contact for the hyperfine interaction as well as the quadrupolar coupling of the vanadium nucleus cannot be achieved with standard DFT methods, even using an expensive basis set. At the current level of theory used for these investigations, the quantum mechanical calculations cannot yield a complete and accurate description of the paramagnetic oxovanadium species, but they can serve as a very useful tool to support the analysis of the experimental spectroscopic data.

Acknowledgment. This work was supported by grant from the NIH (GM 48242 to R.D.B.). The work of M.B. was supported by Swiss National Foundation grant 8220-067593. We thank the Greek General Secretariat Research and Technology (grant 1807/95 to TB) and the Greek Ministry of Education (EPEAEK 2 to Y.D.). We thank Professor Sarah Larsen for the relativistic ADF calculations on the vanadium pentaqua complex.

References and Notes

(1) Eaton, S. S.; Eaton, G. R. In *Vanadium in Biological Systems*; Chasteen, N. D., Ed.; Kluwer Academic Publishers: Boston, 1990; pp 199−222.

(2) Chasteen, N. D. In *Biological Magnetic Resonance*; Berliner, L. J., Reuben, J., Eds.; Plenum Press: New York, 1981; pp 53−119.

(3) Banerjee, A.; Chen, S.; Ruetthard, H.; Jiang, F.; Hu ang, V. W.; Sprinzl, M.; Makinen, M. W. In *Vanadium Compounds: Chemistry, Biochemistry, and Therapeutic Applications*; Tracey, A. S., Crans, D. C., Eds.; ACS Symposium Series Series No. 711; American Chemical Society: Washington, DC, 1998; pp 104−116.

(4) Wever, R.; Krenn, B. E. In *Vanadium Biological Systems*; Chasteen, N. D., Ed.; Kluwer Academic Publishers: Boston 1990; pp 81−98.

(5) Eady, R. R. In *Vanadium Biological System*; Chasteen, N. D., Ed.; Kluwer Academic Publishers: Boston 1990; pp 99−128.

(6) Butler, A.; Walker, J. V. *Chem. Rev.* **1993**, *93*, 1937.

(7) Thompsom, K. H.; McNeil, J. H.; Orivig, C. *Chem. Rev.* **1999**, *99*, 2561.

(8) Crans, D. C.; Keramidas, A. D.; Hoover-Litty, H.; Anderson, O. P.; Miller, M. M.; Lemoine, L. M.; Pleasic-Williams, S.; Vanderberg, M.; Rossomando, A. J.; Sweet, L. J. *J. Am. Chem. Soc.* **1997**, *119*, 5447.

(9) Dubyak, G. R.; Kelinzeller, A. J. *J. Biol. Chem.* **1980**, *255*, 5306.

(10) Schecter, Y.; Karlish, S. J. D. *Nature* **1980**, *284*, 556.

(11) Willsky, G. R.; Goldfine, A. B.; Kostyniak, P. J. In *Vanadium Compounds: Chemistry, Biochemistry, and Therapeutic Applications*; Tracey, A. S., Crans, D. C., Eds.; ACS Symposium Series Series No. 711; American Chemical Society: Washington, DC, 1998; pp 278−296.

(12) Tolis, E. J.; Teberekidis, V. I.; Raptopoulou, C. P.; Terzis, A.; Sigalas, M. P.; Deligiannakis, Y.; Kabanos, T. A. *Chem.*−*Eur. J.* **2001**, *7*, 2698.

(13) Tasiopoulos, A. J.; Troganis, A. N.; Evangelou, A.; Raptopoulou, C. P.; Terzis A.; Deligiannakis, Y.; Kabanos, T. A. *Chem.*−*Eur*. J. **1999**, *5*, 910.

(14) (a) LoBrutto, R.; Hamstra, B. J.; Colpas, G. J.; Pecoraro, V. L.; Frasch, W. D. *J. Am. Chem. Soc.* **1998**, *120*, 4410. (b) Deligiannakis, Y.; Louloudi, M.; Hadjiliadis, N. *Coord. Chem. Rev.* **2001**, *104*, 1.

(15) Fukui, K.; Ohya-Nishiguchi, H.; Kamada, H. *Inorg. Chem.* **1998**, *37*, 2326.

(16) Mustafi, D.; Makinen, M. W. *Inorg. Chem.* **1988**, *27*, 3360.

(17) Grant. C. V.; Ball, J. A.; Hamstra, B. J.; Pecoraro, V. L.; Britt, R. D. *J. Phys. Chem. B* **1998**, *102*, 8145.

(18) Grant, C. V.; Geiser-Bush, K. M.; Cornman, C. R.; Britt, R. D. *Inorg. Chem.* **1999**, *38*, 6285.

(19) Tolis, E. J.; Soulti, K. D.; Raptopoulou, C. P.; Terzis, A.; Sigalas, M. P.; Deligiannakis, Y.; Kabanos, T. A. *Chem. Commun.* **2000**, *7*, 601.

(20) (a) Frisch, M. J.; Trucks, G. W.; Schlegel, H. B.; Scuseria, G. E.; Robb, M. A.; Cheeseman, J. R.; Zakrzewski, V. G.; Montgomery, J. A., Jr.; Stratmann, R. E.; Burant, J. C.; Dapprich, S.; Millam, J. M.; Daniels, A. D.; Kudin, K. N.; Strain, M. C.; Farkas, O.; Tomasi, J.; Barone, V.; Cossi, M.; Cammi, R.; Mennucci, B.; Pomelli, C.; Adamo, C.; Clifford, S.; Ochterski, J.; Petersson, G. A.; Ayala, P. Y.; Cui, Q.; Morokuma, K.; Malick, D. K.; Rabuck, A. D.; Raghavachari, K.; Foresman, J. B.; Cioslowski, J.; Ortiz, J. V.; Stefanov, B. B.; Liu, G.; Liashenko, A.; Piskorz, P.; Komaromi, I.; Gomperts, R.; Martin, R. L.; Fox, D. J.; Keith, T.; Al-Laham, M. A.; Peng, C. Y.; Nanayakkara, A.; Gonzalez, C.; Challacombe, M.; Gill, P. M. W.; Johnson, B. G.; Chen, W.; Wong, M. W.; Andres, J. L.; Head-Gordon, M.; Replogle, E. S.; Pople, J. A. *Gaussian 98*, revision A.7; Gaussian, Inc.: Pittsburgh, PA, 1998. (b) Baerends, E. J.; Autschbach, J. A.; Bérces, A.; Bo, C.; Boerrigter, P. M.; Cavallo, L.; Chong, D. P.; Deng, L.; Dickson, R. M.; Ellis, D. E.; Fan, L.; Fischer, T. H.; Fonseca Guerra, C.; van Gisbergen, S. J. A.; Groeneveld, J. A.; Gritsenko, O. V.; Grüning, M.; Harris, F. E.; van den Hoek, P.; Jacobsen, H.; van Kessel, G.; Kootstra, F.; van Lenthe, E.; Osinga, V. P.; Patchkovskii, S.; Philipsen, P. H. T.; Post, D.; Pye, C. C.; Ravenek, W.; Ros, P.; Schipper, P. R. T.; Schreckenbach, G.; Snijders, J. G.; Sola, M.; Swart, M.; Swerhone, D.; te Velde, G.; Vernooijs, P.; Versluis, L.; Visser, O.; van Wezenbeek, E.; Wiesenekker, G.; Wolff, S. K.; Woo, T. K.; Ziegler, T. *ADF2002.03*; SCM, Theoretical Chemistry, Vrije Universiteit: Amsterdam, The Netherlands; http://www.scm.com.

(21) Flükiger, P.; Lüthi, H. P.; Portmann, S.; Weber, J. *MOLEKEL 4.3*; Swiss Center for Scientific Computing: Manno, Switzerland, 2000−2002.

(22) Bailey, W. C.; Gonzalez, F. M.; Castiglione, J. *Chem. Phys.* **2000**, *260*, 327.

(23) Bailey, W. C.; Gonzalez, F. M. *J. Mol. Struct.* **2003**, *689*, 651.

(24) Wu, G.; Wong, A.; Wang, S. *Can. J. Chem.* **2003**, *81*, 275.

(25) Bryce, D. L.; Wasylishen R. E. *J. Phys. Chem. A* **1999**, *103*, 7364.

(26) Liu, T.; Lowell, T.; Han, W.-G.; Noodleman, L. *Inorg. Chem.* **2003**, *42*, 5244.

(27) Elmi, F.; Hadipour, N. L.; Safinezhad, F. *Chem. Phys. Lett.* **2003**, *375*, 273.

(28) Kim, S. H.; Aznar, C. P.; Brynda, M.; Silks, L. A. P.; Michalczyk, R.; Unkefer, C. J.; Woodruff, W. H.; Britt, R. D. B. *J. Am. Chem. Soc.* **2004**, *126*, 2328.

(29) Saladino, A. C.; Larsen, S. C. *J. Phys. Chem. A* **2002**, *106*, 10444.

(30) Pooransingh, N.; Pomerantseva, E.; Ebel, M.; Jantzen, S.; Rehder, D.; Polenova, T. *Inorg. Chem.* **2003**, *42*, 1256.

(31) Pyykko, P.; Seth, M. *Theor. Chem. Acc.* **1997**, *96*, 92.

(32) Ehmann, J.; Fähnle, M. *Phys. Rev. B* **1997**, *55*, 7478.

(33) Sturgeon, B. E.; Britt, R. D. *Rev. Sci. Instrum.* **1992**, *63*, 2187.

(34) Strugeon, B. E.; Britt, R. D. *J. Phys. Chem.* **1994**, *98*, 12871.

(35) Davies, E. R. *Phys. Lett.* **1974**, *47A*, 1.

(36) Grant, C. V.; Cope, W.; Ball, J. A.; Maresch, G. G.; Gaffney, B. J.; Fink, W.; Britt, R. D. *J. Phys. Chem. B* **1999**, *103*, 10627.

(37) Nilges, M. J. Ph.D. Thesis, University of Illinois, Urbana, Illnois, 1979.

(38) Belford, R. L.; Nilges, M. J. *Computer Simulation of Powder Spectra*; Presented at the International Electron Paramagnetic Resonance Symposium, Twenty First Rocky Mountain Conference, Denver, Colorado, 1979.

(39) Maurice, A. M., Ph.D. Thesis, University of Illinois, Urbana, Illinois, 1980.

(40) Da Silva, J. J. R. F.; Wootton, R. *Chem. Commun.* **1969**, *1*, 3175.

(41) Caira, M. R.; Haigh, J. M.; Nassimbeni, L. R. J. *Inorg. Nucl. Chem.* **1972**, *34*, 3171.

(42) Selbin, J. *Coord. Chem. Rev.* **1966**, *1*, 293.

(43) Ashby, C.; Cheng, C. P.; Brown, T. *J. Am. Chem. Soc.* **1978**, *1*, 6057.

(44) Ida, R.; Wu, G. *J. Phys. Chem. A* **2002**, *106*, 11234.

(45) Chentit, M.; Sidorenkova, H.; Geoffroy, M.; Ellinger, Y. *J. Phys. Chem. A* **1998**, *102*, 10469.

(46) Saladino, A. C.; Larsen, S. C. *J. Phys. Chem. A* **2003**, *107*, 1872.

(47) Munzarova, M. L.; Kubacek, P.; Kaupp, M. *J. Am. Chem. Soc.* **2000**, *122*, 11900.

(48) Munzarova, M.; Kaupp, M. *J. Phys. Chem. A* **1999**, *103*, 9966.

(49) BHandHLYP functionals include HF, LSDA, and Becke's exchange functionals as well as the LYP correlation functional of Lee, Yang, and Parr with the following parameters: $0.5*E_X^{HF} + 0.5*E_X^{LSDA} + 0.5*E_X^{Becke88} + E_C^{LYP}$.

(50) The corresponding values calculated with BHandHLYP and 6-311++g basis sets are $\Delta A_{zz\ calcd} = 32$ and 34 MHz for Cl^- and SCN^-; $\Delta A_{iso\ calcd} = 25$ and 28 MHz; and $\Delta_{spin} = 0.013$ and 0.002 for Cl^- and SCN^-, respectively. This indicates that the interpretation of the Mulliken spin densities should be performed with particular care, especially with the species in which spin polarization is important.

(51) Ballhausen, C. J.; Gray, H. B. *Inorg. Chem.* **1962**, *1*, 111.